Mesoscale variability off California as seen by the GEOSAT altimeter

P. FLAMENT (Department of Oceanography, University of Hawaii at Manoa, Honolulu HI 96822)

P.M. KOSRO and A. HUYER (College of Oceanography, Oregon State University, Corvallis OR 97331)

Abstract. GEOSAT altimeter data was used to study the seasonality, spatial distribution and propagation of mesoscale features in the California Current. Relative topography from the altimeter was first compared with dynamic topography from collinear hydrographic sections. After removing a mean offset, the rms difference was 3-4 cm, barely more than the noise of the altimeter. Statistics of relative topography variability were then estimated over 19 months. Variability reaches 10-12 cm rms near the coast off Northern California, Point Conception, and Point Eugenia. High variability off Northern California extends offshore as two bands ~200 km wide, one towards the southwest, the other one towards the west following the Mendocino escarpment. It decreases westward reaching the background of 4 cm rms at 600 km from the coast. It also decreases to ~4 cm rms north of 42°N and south of 26°S, even near the coast. Time-latitude correlations show poleward propagation of sea level anomalies at about 4 km/day for the two tracks closest to shore, but not further offshore. Rms alongshore topography between 30°N and 40°N has a marked seasonal cycle. Close to shore, it is smallest in fall and winter, and largest during the upwelling season. The cycle lags by ~0.5 day/km and decreases in amplitude westward; it is not detected further than ~500 km offshore. This suggests that mesoscale variability in the California Current is dominated by the growth and seaward migration of meanders of the upwelling front, dynamically linked to the wind-driven coastal upwelling cycle. (California Current, mesoscale eddies, altimeter).

1. Introduction

The summertime mesoscale flow off Central and Northern California consists of large meanders of the California Current. The seaward branches of the meanders are ~40 km-wide baroclinic jets that transport about $2 \cdot 10^6 m^3/s$ of cold water westward from the coastal upwelling region. They appear on satellite infrared images as cold filaments that extend up to 400 km offshore and are generally referred to as upwelling filaments (Brink, 1983, 1987). The structure of these meanders in spring and summer is well known off Point Arena (39°N) and off Point Conception (34°N), having been studied in numerous field programs (Rienecker *et al.*, 1985; Flament *et al.*, 1985; Kosro and Huyer, 1986; Barth and Brink, 1987; Coastal Transition Zone Group, 1988). However, little is known of the structure of the flow at other locations, and at other times of the year.

Our objective in this paper is to study the spatial distribution, the propagation and the seasonality of these mesoscale features along the West coast of North America, from 20°N to 50°N, using ocean surface topography from the GEOSAT altimeter. Because neither the orbit of GEOSAT nor the absolute geoid currently are known with sufficient accuracy, only a variability study can be made in low energy regions such as this one: the mean flow is not presently accessible.

The data and the processing steps followed are described in section 2. The altimeter-derived ocean topography is compared with two collinear hydrographic sections in section 3. The spatial distribution of relative topography variability is presented in section 4 and the temporal distribution in section 5. Possible sources of errors are addressed in section 6.

2. Data and processing

The GEOSAT Exact Repeat Mission provides repeated collinear profiles of sea surface elevation every 17 days with along-track resolution of 7.3 km. The ascending tracks are nearly parallel to the coast of California, and, at the latitude of Point Arena, are found at 85, 215, 345, 475,... km offshore (Fig. 1). Only ascending tracks were processed for this study because many cycles of the descending tracks are missing (Nov. 1986 to Feb. 1987 and Nov. 1987 to Feb. 1988), making it difficult to resolve the seasonal upwelling cycle unambiguously.

The data were processed for the period November 1986 to April 1988 (19 months, 34 repeat cycles). One-second averaged altimeter heights were corrected for ocean and earth tides, water vapor (FNOC), tropospheric (FNOC) and ionospheric delays, and surface pressure (FNOC) using the corrections given on the NOAA tapes. Orbit errors were modeled as parabolas over 30° arcs and removed. Each profile was then linearly interpolated to a common grid and the average geoid was subtracted to obtain relative surface topography $h(\lambda,t)$, where λ is the latitude and t is the time of each repeat cycle. This procedure removes both the mean and any ~30°-scale oceanic signals.

The along-track power spectrum of relative topography for the track closest to the coast is shown in Fig. 2, normalized by a 3-cm rms gaussian white noise. It is red at wavenumbers smaller than 1/50 km^{-1} but has a white shape due to instrument noise at higher wavenumbers (the drop of power near the high wavenumber end is caused by the interpolation, *cf.* Fu, 1983). Because noise dominates at short wavelengths, relative topography was filtered by a running mean over 7 samples (50 km). The contribution of wavelengths longer than 50 km to noise is ~1.2 cm rms.

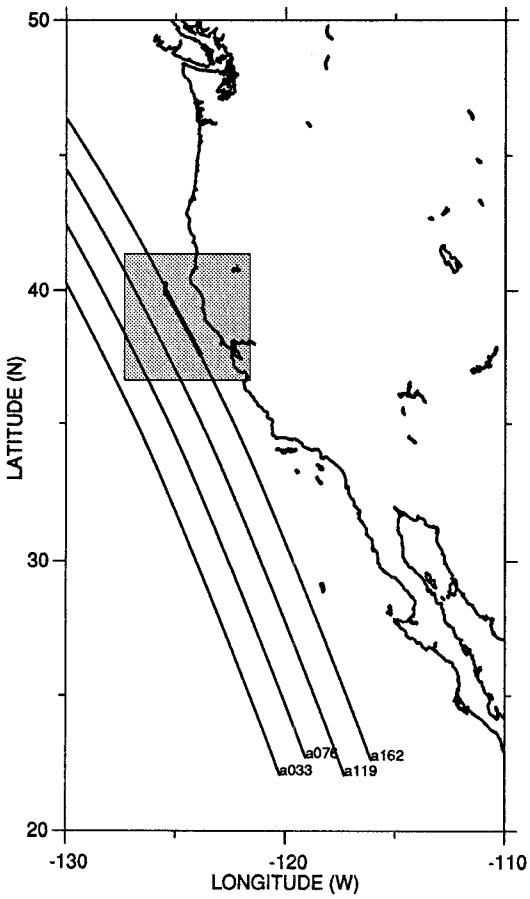

Fig. 1. Map of the area studied, showing the four GEOSAT ascending tracks nearest shore: a162, a119, a076 and a033. The position of the satellite image shown in Fig. 4 is outlined.

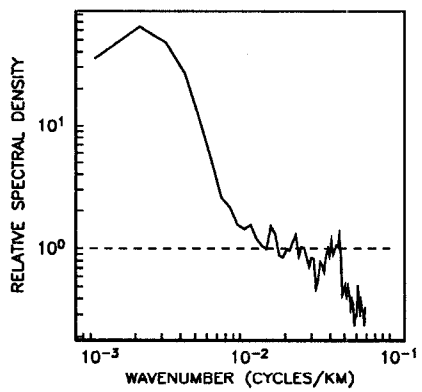

Fig. 2. Along-track power spectrum of relative topography for track a162, normalized by a 3-cm white noise.

3. Comparison with hydrography

A line of CTD hydrographic stations surveyed in May and June 1987 (Schramm *et al.* 1988a, 1988b) coincided with the ascending track closest to the coast. The stations were spaced ~15 km apart. The dynamic topography referenced to 500 dbar was computed and, for each survey, the mean over the length of the section was subtracted. The unfiltered altimeter topography was then interpolated in space and time to the positions of the stations, and, for each survey, the mean over the length of the section was also subtracted.

These relative surface topographies are shown in Fig. 3. In May and June, the altimeter clearly shows the 20 cm signal due to the meander of the California Current seen near 39°N in the AVHRR image of 16 June at 2300 UT (Fig. 4). The topography corresponds to an offshore speed of about ~0.50 m/s over a width of ~30 km. The rms differences between the relative topographies determined from the altimeter and from the CTD sections are 3.3 and 4.2 cm for the May and June surveys. The two topographies are in remarkable agreement, given the ~3-cm rms noise of the radar altimeter (Cheney *et al.*, 1989; Sailor and LeSchack, 1987).

These results show that the altimeter topography is capable of resolving the mesoscale structure of the California Current. They also indicate that, over the period analyzed, the meander was intermittent (if it were a steady feature, its surface expression would be removed with the mean and would not appear in the relative topography), and that the barotropic component was small at this spatial scale, the hydrographic reference level of 500dbar capturing most of the flow (Kosro and Huyer, 1986).

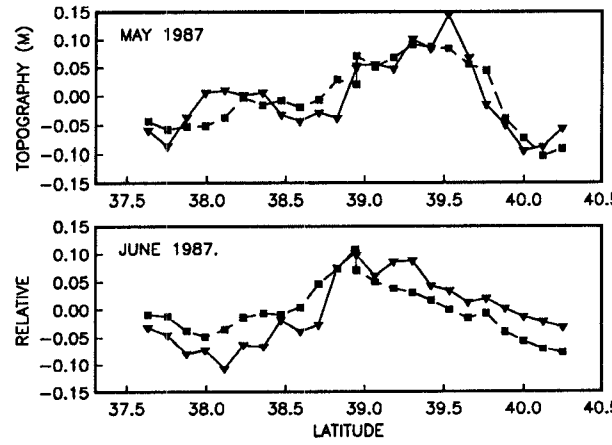

Fig. 3. Comparison between relative topography from the altimeter (dotted line, □) and from hydrography (solid line, ∇); see text.

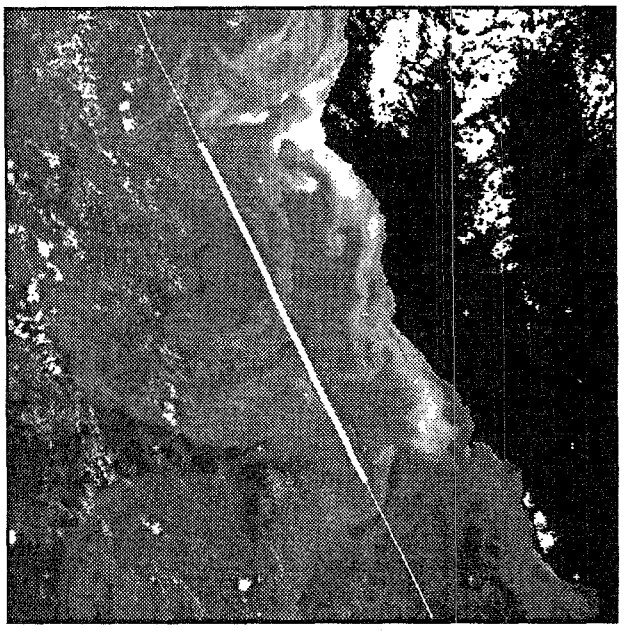

Fig. 4. Thermal infrared AVHRR image on 16 June 1987 at 23:00 UT. Cold water is coded in white and warm water in black. GEOSAT track a162 is shown, with the segment coinciding with the CTD surveys as a thick line.

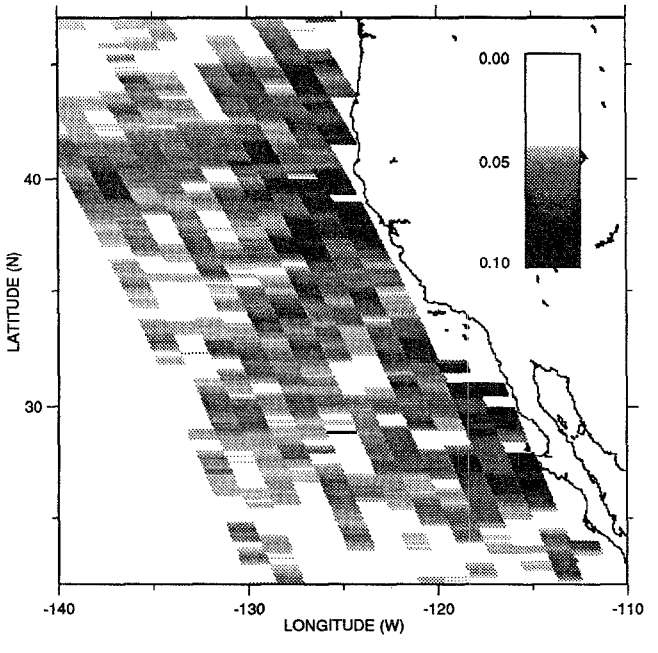

Fig. 5. Map of variability of relative topography over the Eastern Pacific, gray-coded from white (0.00 m rms) to black (0.10 m rms).

4. Spatial distribution of variability

Variability of relative topography, defined as $T^{-1}\int_0^T dt\, h(\lambda,t)^2$, was computed over the Eastern Pacific for the first 18 months of the mission, and is displayed in Fig. 5 by assigning gray-coded values of variability to rectangular pixels 7.3 km in latitude by 130 km in longitude. Variability along the three ascending tracks closest to the coast is also plotted as function of latitude in Fig. 6. Based on the sample size of 34, the 90% confidence limits are (7,10) cm for a variability of 8 cm rms.

Marked enhancements of variability are seen near the coast of California, reaching 10-12 cm rms west of Point Reyes/Point Arena/Cape Mendocino, south of Point Conception, and around Point Eugenia (Baja California). Variability decreases progressively towards offshore to a typical background value of 4 cm rms at ~600 km from the coast. Variability decreases rapidly to this background value north of 42°N and south of 26°S, even near the coast. Spatial patterns of variability are apparent. The region of high variability off Northern California extends offshore as two bands ~200 km wide, one towards the west following nearly exactly Mendocino escarpment at 40°N, the other one towards the southwest. This region is separated from the one south of Point Conception by a band of low variability, starting surprisingly close to the coast.

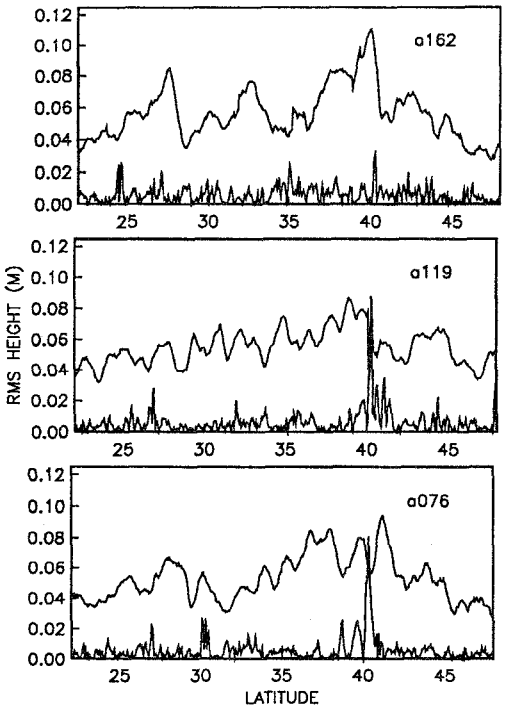

Fig. 6. Variability along the three ascending tracks nearest shore as function of latitude. Also shown is the rms longitude deviation from the exact repeat track, scaled by the along-track geoid slope.

Variability is enhanced in areas where meanders of the California Current have been observed previously. High variability off Baja California suggests the occurrence of similar meanders and filaments there. The band of low variability off Central California is a surprise. A strong offshore jet has been observed at that location in July 1984 (Chelton *et al.*, 1987) and July 1985 (Flament and Armi, 1989). Is this jet intermittent, so that this study is based on time series too short to be considered stationary? Or is this jet steadier than those off Northern California, leading to less variability of relative topography?

5. Propagation of features and temporal variations

Two-dimensional time-latitude correlation functions of $h(\lambda,t)$ are shown in Fig. 7 for the three ascending tracks near the coast. Along-track propagation of sea level anomalies at about 4 km/day poleward is evident for the two tracks nearest shore, but not further offshore. A similar northwestward propagation speed has been reported by Flament and Armi (1989), who observed the translation at ~4.7 cm/s of the root of an offshore jet near 36°N, using repeated hydrographic sections and sequences of satellite infrared images. However, there have also been reports of southward motion (e.g. Flament *et al.*, 1985).

Contours of relative topography as a function of λ and t are shown in Fig. 8 for the three ascending tracks near to the coast. Along the track nearest the coast (a162, 85 km from Point Arena), sea level drops sharply in mid-April and stays low throughout the spring and summer, i.e. throughout the upwelling season. Along the second offshore track (a119, 215 km from Point Arena), sea level is also low in summer and early fall, but the lowest levels are not seen until September. Along the third offshore track, (a076, 345 km from Point Arena), low sea levels are not seen until winter, and do not appear to be more persistent than high sea levels. These data, together with the hydrographic surveys, suggest that the lows in sea level are regions inshore of an upwelling front, which forms on the shelf in early spring and subsequently moves offshore.

Along-track variability, defined as $\Delta\lambda^{-1} \int_{\lambda_0}^{\lambda_0+\Delta\lambda} d\lambda\, h(\lambda,t)^2$, was also computed for each track over the latitude band 30°N to 40°N, and is shown in Fig. 9 gray-coded as a function of time and of the longitude at which each track crosses 35°N. The 6-cm rms contour is outlined in white; dark areas correspond to larger values (up to 12-cm rms for black), light areas to smaller values. This plot is somewhat noisy, but nevertheless show a seasonal cycle. Along the track nearest the coast, along-track variability is smaller than 6 cm rms from late fall to late winter, and larger than 6 cm rms in spring and summer. The time at which along-track variability increases in spring occurs later further offshore, with a delay of ~0.5 day/km. The seasonal cycle decreases in amplitude towards offshore, and is not detected further than 129°W (~500 km from the coast). Removing for each track the mean sea level over the same latitude band does not modify significantly the contour plot, indicating that most of the along-track variability signal is due to the offshore jets at a scale of a few hundreds of kilometers and not to larger scale seasonal variations of sea level.

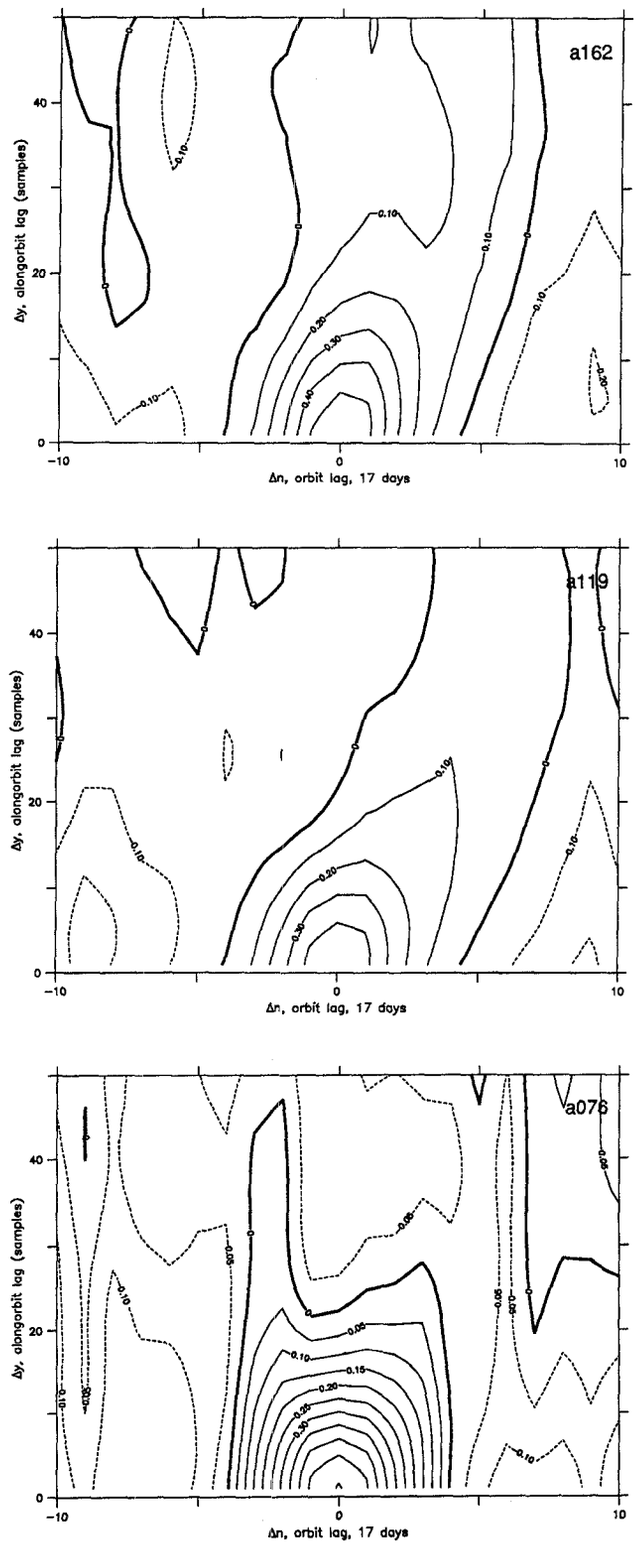

Fig. 7. Two-dimensional time-latitude correlation functions for tracks a162, a119 and a076. Lag units are in cycles (17 days) on the x axis and along-track samples (7.3 km) on the y axis.

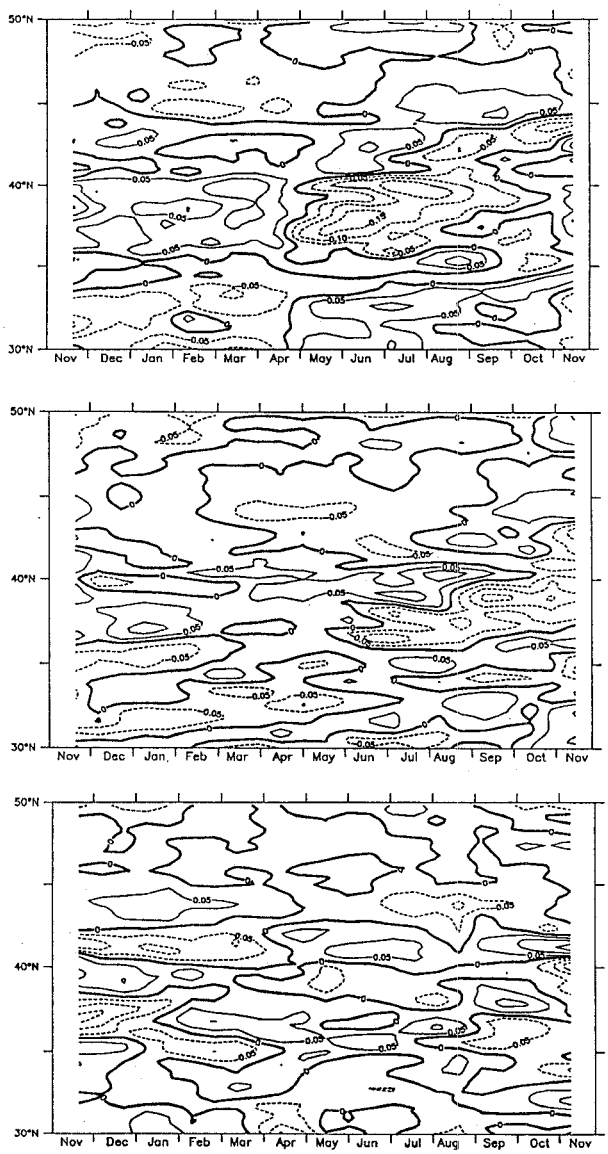

Fig. 8. Contours of relative topography as a function of time and latitude for tracks a162, a119 and a076. Negative levels are dashed.

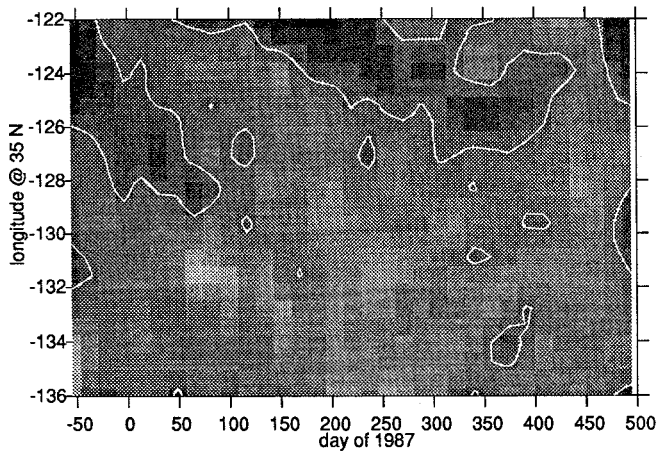

Fig. 9. Average along-track variability between 30°N and 40°N as a function of time and longitude at which each track crosses 35°N. The 6 cm rms contour is outlined. Darker areas correspond to larger values, lighter ones to smaller values.

6. Sources of errors

The principal sources of contamination are water vapor in the troposphere, cross-track geoid slopes and electro-magnetic bias. As will be shown below, none of them seem to be sufficient to affect the patterns presented above.

The weakest correction is for microwave propagation delay due to water vapor in the troposphere. The correction provided on the tapes is derived from the 2.5°-resolution FNOC atmospheric model. It is of the order of 12 cm in this area, and varies by ±6 cm, but on scales larger than the patterns of variability seen in Fig. 5. Fu (1983) presented power spectra of water vapor correction and surface topography, based on simultaneous SEASAT SMMR and altimeter data in low mesoscale energy areas, which showed a signal-to-correction ratio ranging from 12 dB at scales of 100 km to 4 dB at 1000 km.

Plots of rms longitude deviation from the exact repeat track, scaled by the along-track geoid slope, are shown with the plots of rms variability in Fig. 6 to provide a crude estimate of contamination by unknown small-scale cross-track geoid slopes, which can be large near seamounts and fracture zones. In particular, the Mendocino escarpment near 40°N contributes significantly to rms variability of the surface, and it is not clear whether the region of enhanced variability along 40°N is entirely real, or is in part an artifact due to cross-track deviations over the escarpment. Except for isolated seamounts, bottom topography is fairly regular further south and does not affect the patterns of variability.

Electro-magnetic bias is a wave-height dependent correction due to stronger reflection of the radar signal by the troughs than by the crests of asymmetric finite amplitude surface waves. It was not applied here. For GEOSAT, it is ~-1% of significant wave height $H_{1/3}$ (Cheney *et al.*, 1988). Over the Eastern Pacific, $H_{1/3}$ measured by GEOSAT increases progressively from 2 m at 25°N to 4-5 m at 45°N, with little structure at scales of 1000 km or less. Most of the EM bias is thus removed with the parabolic orbit error.

7. Summary and conclusions

A mesoscale meander observed in the hydrography was also found in the altimeter topography. The measurements agreed to ~3-4 cm rms, showing that the GEOSAT altimeter is capable of resolving the mesoscale structure of the California Current.

The altimeter data showed that sea level variability is enhanced two to three-fold within 500 km from the coast of North America compared to the offshore background level. The strength of the variability varied also along the coast and peaked where strong meanders and westward jets have been found recurrently, suggesting that nearshore variability of relative topography can be attributed primarily to these meanders and jets.

Variability is modulated seasonally, suggesting that these jets are dynamically linked to the coastal upwelling cycle, and that the corresponding cold filaments observed in satellite images may not be simply the expression of colder nearshore water passively advected in a background field of offshore eddies.

The ~500 km offshore extension of high variability in sea level could be used as a definition of the Coastal Transition Zone. It is larger than the typical ~300 km extension of cold filaments seen in AVHRR images, indicating that the surface temperature expression of a filament disappears closer to shore than does the kinetic energy of the jet.

References

Coastal Transition Zone Group, "The Coastal Transition Zone Program," *EOS, Trans. Am. Geophys. Union*, vol. 69, no. 27, p. 698ff (1988).

Barth, J. A. and K. H. Brink, "Shipboard acoustic doppler profiler velocity observations near Point Conception: spring 1983," *J. Geophys. Res.*, vol. 92, pp. 3925-3943 (1987).

Brink, K.H., "The near-surface dynamics of coastal upwelling," *Prog. Oceanog.*, vol. 12, pp. 223-257 (1983).

Brink, K.H., "Coastal ocean physical processes," *Rev. Geophys.*, vol. 25, pp. 204-216 (1987).

Chelton, D. B., R. L. Bernstein, A. Bratkovich, and P. M. Kosro, "The Central California Coastal Circulation Study," *EOS, Trans. Amer. Geophys. Union*, vol. 68, no. 1, p. 1ff (1987).

Cheney, R.E., B.C. Douglas, and L. Miller, "Evaluation of GEOSAT altimeter data with application to tropical Pacific sea level variability," *J. Geophys. Res.* (1989). (in press)

Cheney, R.E., J.G. Marsh, and B.D. Beckley, "Global mesoscale variability from collinear tracks of SEASAT altimeter data," *J. Geophys. Res.*, vol. 88, p. 4343 (1983).

Flament, P. and L. Armi, "Observations of surface convergence, subduction and related finestructure," *J. Geophys. Res* (1989). (submitted)

Flament, P., L. Armi, and L. Washburn, "The evolving structure of an upwelling filament," *J. Geophys. Res.*, vol. 90, pp. 11,765-11,778 and 11,835-11,836 (1985).

Fu, L.L, "On the wave number spectrum of oceanic mesoscale variability observed by the SEASAT altimeter," *J. Geophys. Res.*, vol. 88, pp. 4331-4342 (1983).

Kosro, P.M. and A. Huyer, "CTD and velocity surveys of seaward jets off Northern California," *J. Geophys. Res.*, vol. 91, pp. 7680-7690 (1986).

Rienecker, M., C.N.K. Mooers, D.E. Hagan, and A.R. Robinson, "A cool anomaly off Northern California: an investigation using IR imagery and in situ data," *J. Geophys. Res.*, vol. 90, pp. 4807-4818.

Sailor, R.V. and A.R. LeSchack, "Preliminary determination of the GEOSAT altimeter noise spectrum," *Johns Hopkins APL Tech. Digest*, vol. 8, no. 2, pp. 182-183 (1987).

Sailor, R.V. and A.R. LeSchack, "Preliminary determination of the GEOSAT altimeter noise spectrum," *Johns Hopkins APL Tech. Digest*, vol. 8, no. 2, pp. 182-183 (1987).

Schramm, Richard E., Jane Fleischbein, Adriana Huyer, P. Michael Kosro, Tim Cowles, and Nan Dudek, "CTD Observations in the Coastal Transition Zone off Northern California, 9-18 June 1987," Ref. 88-3, College of Oceanography, Oregon State University, Corvallis, 1988b.

Schramm, Richard E., Jane Fleischbein, Robert Marsh, Adriana Huyer, P. Michael Kosro, Tim Cowles, and Nan Dudek, "CTD Observations in the Coastal Transition Zone off Northern California, 18-27 May 1987," Ref. 88-3, College of Oceanography, Oregon State University, Corvallis, 1988a.

Acknowledgements. We would like to thank M. Caruso, S. Gille and Z. Sirkes, who assisted with the development of GEOSAT processing software, and D. Kelley for providing an outstanding plotting package. This work was partially supported by the Office of Naval Research through contracts N000014-87-K-007, N00014-87-K-0242 and N00014-86-K-0751, and grant N00014-89-J-1599.